THE JOURNAL OF PHYSICAL CHEMISTRY A

 VOLUME 105, NUMBER 15, APRIL 19, 2001

LETTERS

Homogeneity, Transport, and Signal Properties of Single Ag Particles Studied by Single-Molecule Surface-Enhanced Resonance Raman Scattering

C. Eggeling,[†] J. Schaffer,[†] C. A. M. Seidel,*[,†] J. Korte,[‡] G. Brehm,[‡] S. Schneider,*[,‡] and W. Schrof[§]

Max-Planck Institut für Biophysikalische Chemie, Am Fassberg 11, D-37077 Göttingen, Germany, Institut für Physikalische und Theoretische Chemie, Universität Erlangen−Nürnberg, Egerlandstrasse 3, D-91058 Erlangen, Germany, and Department of Polymer and Solid State Physics, ZKM, BASF-AG, D-67056 Ludwigshafen, Germany

Received: July 19, 2000; In Final Form: January 8, 2001

We extended the sensitivity of Raman correlation spectroscopy in solution to the single-molecule level by applying surface- and resonance-enhanced Raman scattering (SERRS) combined with time-gated, confocal signal detection. The brightness of the SERRS signal of single Rhodamine 6G molecules adsorbed on a single silver nanoparticle is comparable to fluorescence. Rare event analysis reveals the existence of few particles with simultaneous SERRS and fluorescence signal. The observation of a dynamic exchange between heterogeneous binding sites is supported by the existence of multiple SERRS brightnesses in the signal intensity distribution and by signal fluctuations in the 60 μs time range detected by autocorrelation analysis. Finally, polarization-dependent SERRS autocorrelation curves and single-particle analysis allowed us to measure individual rotational diffusion times and to directly analyze the heterogeneity of the ensemble in solution.

Introduction

Recent advances in ultrasensitive instrumentation have allowed the detection of single molecules and particles under both cryogenic and ambient conditions by various optical methods such as absorption,[1] fluorescence[2] or surface- and resonance-enhanced Raman scattering (SERRS) spectroscopy.[3−5] To achieve single-molecule sensitivity, a microscope is used for laser excitation and collection of signal. Raman spectroscopy is a valuable method for single-molecule studies because of the high chemical information content obtained by the characteristic fingerprint of its vibrational spectrum. Thereby, spectra are generated on a spectrograph, and the dispersed signal is usually registered by a slow-scan or intensified CCD camera with a long-term frame rate ≤50 Hz. This substantially limits the time-resolution of these measurements to 20 ms or slower.

In the last three decades, optical fluctuation spectroscopies have become indispensable tools to characterize dynamic phenomena. In combination with a confocal microscope, fluorescence correlation spectroscopy (FCS) studies particles and molecules at nanomolar concentrations via characteristic signal fluctuations.[6−9] FCS can monitor ligand receptor interactions via changes of translational or rotational Brownian motion and characterizes a wide range of chemical reactions and photophysical processes. Using an array of avalanche photodiodes (APDs) with a dead time below 1 μs, correlation spectroscopy based on Raman scattered light was recently successfully applied to study the Brownian motion of aggregates

* To whom correspondence should be addressed. E-mail: cseidel@gwdg.de. Phone: ++49/551/201−1774. Fax: ++49/551/201−1006. E-mail: schneider@ pctc.chemie.uni-erlangen.de.
[†] Max-Planck Institut für Biophysikalische Chemie.
[‡] Universität Erlangen−Nürnberg.
[§] Department of Polymer and Solid State Physics, ZKM, BASF-AG.

10.1021/jp002552+ CCC: $20.00
Published on Web 03/28/2001

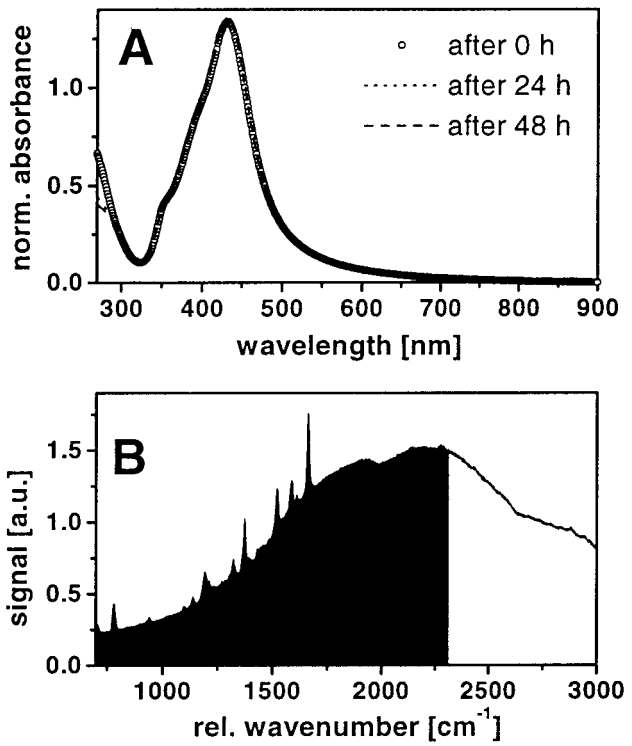

Figure 1. (A) Salt dependence of absorption spectrum of a monodisperse silver colloid with 43 ± 6 nm diameter, whose absorption maximum is shifted 20 nm to shorter wavelengths compared to Ag54. Starting condition[20,22] (0 h): 10^{-4} M aqueous Ag(0) solution containing no KCl. No change of the absorbance is observed 24 and 48 h after the KCl concentration of the solution was increased to 2 mM. (B) SERRS spectrum (excitation wavelength 496.5 nm) of a bulk measurement of a Ag54 solution containing 100 nM Rhodamine 6G. Superimposed on the broad fluorescence spectrum sharp peaks of the SERRS signal are detectable. The black shaded area corresponds to the spectral window of the band-pass filter used in the single-particle measurements.

of multiple dyes with diameters of several hundred nanometers.[10] The prerequisite for such a study is, however, that the scatterer exhibits a very large Raman cross-section and low fluorescence quantum yield. To overcome these restrictions, we will use the phenomenon of SERRS.[11] Recent publications[3,5,12−14] demonstrated that SERRS and surface-enhanced Raman scattering (SERS) can be recorded even from a single molecule with an effective cross-section of approximately 10^{-16} cm^2. However, there is an ongoing debate about the heterogeneity of binding sites and the importance of the various factors on the enhancement such as particle size, electronic resonance, chemical bonding and electromagnetic field magnification.[11,15] In one case, SERRS signals were recorded from single, immobilized silver particles,[3] whereas in solution, a cluster of freely diffusing particles was claimed to be necessary for sufficient enhancement.[5] More recent publications seem to indicate that particle association may help to generate an ultrahigh amplification factor,[4] although aggregation is, in our opinion, not the only decisive parameter. This view is supported by recent calculations applying SERS quadrupole theory.[16]

To perform SERRS correlation spectroscopy with high time resolution, we decided to use methods usually applied in single-molecule multiparameter fluorescence detection (MFD).[17,18] Using two APDs and excitation with 200 ps laser pulses, multiparameter fluorescence spectroscopy simultaneously measures three parameters of the signal with a high macroscopic time resolution (400 ns): (i) intensity, (ii) decay time by time-correlated single-photon counting (TCSPC), and (iii) polarization. Thereby, the total signal of the sample in a spectral range of 550−2300 cm^{-1} rel. wavenumbers is detected, but "software" time-gating with 50 ps time channels allows us to separate the temporally prompt SERRS signal from the in part spectrally overlapping delayed fluorescence signal.

In this letter we will provide direct evidence that single Rhodamine 6G (Rh6G) molecules adsorbed on a single silver nanoparticle in solution are sufficient to generate an intensity of a SERRS signal comparable to that of fluorescence. Furthermore, we investigate temporal fluctuations of the SERRS signal and characterize different categories of adsorption sites on the metal surface with respect to their fluorescence and SERRS properties. Finally, we will demonstrate the measurement of single-particle rotational correlation times.

Material and Methods

Sample. Two different types of silver particles were investigated: (i) nearly spherical, essentially monodisperse particles (Ag54) with 54 ± 6 nm diameter (≈10^{13} particles/L) and a characteristic FCS diffusion time $\tau_D = 20$ ms[6] (preparation refs. 19 and 20) and (ii) polydisperse particles (AgLM) prepared according to the protocol of Lee and Meisel and reported by Hildebrandt and Stockburger.[21] The silver hydrosols were activated by Cl^--ions (2 mM) and incubated for 12 h with a dilute solution (10^{-12} M) of Rh6G. This procedure led to an average coverage of less than one dye molecule per silver particle.

The advantage of using monodisperse silver colloid is twofold: (i) Because of the narrow distribution in size and shape as proven by transmission electron microscopy,[22,23] the extinction spectra exhibit fairly narrow bands whose maxima are characteristic for particle size (Figure 1A). Furthermore, the changes induced in the extinction spectra by dimer, trimer, and higher aggregate formation can easily be seen and used as criterion for estimating the extent of aggregation. (ii) Stabilization of the colloid against aggregation can be achieved by overcompensating the attractive van der Waals dispersion forces by repulsive Coulomb interaction of the electrical double layer created by adsorbed anions (Cl^-). In the case of colloids with a wide range of particle sizes and forms, the net interaction is most likely different for each pair of particles leading to the formation of an even more heterogeneous sample (e.g., only particles of a certain size aggregate).

Upon addition of salt and solute to the monodisperse colloid, as described above, we did not observe changes in the extinction spectra over days (Figure 1A). This can be taken as strong evidence that the fraction of aggregated particles must be below 5%. Nevertheless, good SERRS spectra of an ensemble can be recorded from dye solutions containing as little as 10^{-8} M Rhodamine 6G (Figure 1B).

Measurement Technique. Using this preparation procedure, a heterogeneous sample with free and adsorbed dye molecules is obtained. The application of SERRS implies that the fluorescence of chromophores not bound to the surface can, in principle, contribute to the recorded signal, because it can spectrally overlap with the Raman scattered light. In our case, excitation below 500 nm allows us to cut off half of the fluorescence of the free dye (the fluorescence of the adsorbed dye is efficiently quenched by excitation transfer to the metal surface) by applying a band-pass filter covering the frequency range 550−2300 cm^{-1} (black areas in Figure 1B). At the same time, this filter suppresses the Rayleigh scattered light.

However, conventional correlation spectroscopy, which uses the total signal of the ensemble, is not appropriate, because it lacks sensitivity and molecular selectivity. Selective analysis

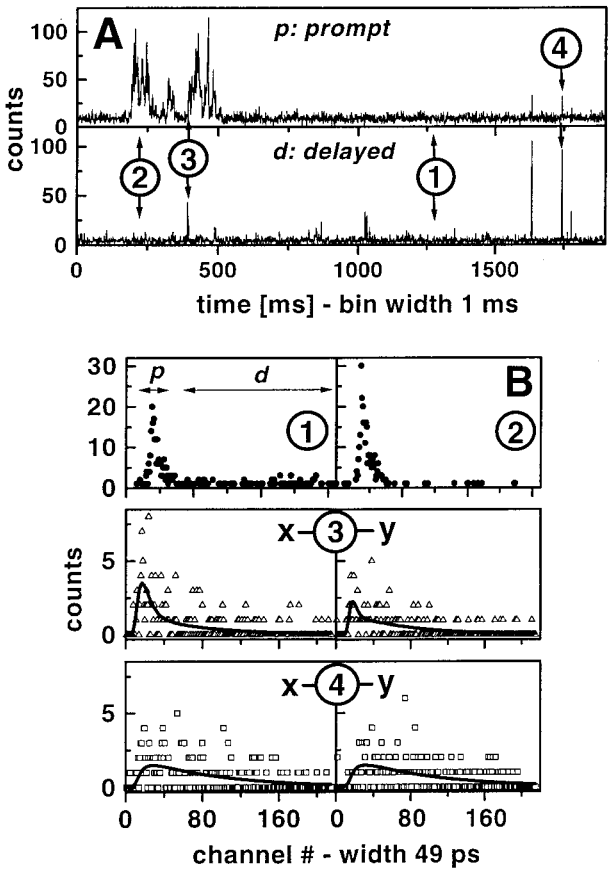

Figure 2. (A**)** Multichannel scaler traces of the sample Ag54 obtained by time gated signal detection (prompt *p*, delayed *d*). The assigned time channels are indicated by arrows in the arrival time histogram 1 (part B). (B**)** Arrival time histograms at marked positions in the traces of part A: (1) 300 photons of background signal (empty channels contain no symbol), (2) SERRS signal (empty channels contain no symbol), and (3) and (4) decays of the parallel (x) and perpendicular (y) polarized signal components with fit curves. Fit of 3 yields for bound Rh6G (triangles) $\tau = 2.9 \pm 0.35$ ns, $\rho = 0.7 \pm 0.1$ ns, $r = 0.08$, and $\gamma = 0.36$. Fit of 4 yields for free Rh6G (squares) $\tau = 4.1 \pm 0.35$ ns, $\rho = 0.2 \pm 0.1$ ns, $r = 0.02$, and $\gamma = 0.03$ (for explanations of parameters see text).

of certain molecular species is only possible by single-molecule spectroscopy. MFD based on the recently developed BIFL technique (burst integrated fluorescence lifetime)[17,18] can surmount this problem by characterizing directly individual members of the ensemble in a highly diluted sample solution (average particle number in the detection volume <0.1) and subjecting members of certain species to subsequent selective analysis.

Setup. Single-molecule SERRS was performed with a confocal epi-illuminated microscope with two detectors for separate detection of parallel or perpendicular polarized signal components [pinhole 100 μm, polarization beam splitter cube (VISHT11), spectral band-pass filter (rel. wavenumbers 550−2300 cm^{-1}), detection volume of 3 fl (characteristic FCS diffusion time of Rh6G in water, $\tau_D = 0.3$ ms)].[18] A linear polarized, mode-locked argon ion laser was applied for pulsed excitation at 496 nm (repetition rate 73 MHz, pulse width 190 ps, focal excitation irradiance 190 kW cm^{-2}). The detected photons were registered by a PC−BIFL card (SPC 432, Becker & Hickl GmbH, Berlin, Germany) in a list mode. The stored data were subjected to selective analysis as described below.

Results and Discussion

Measurement and Data Analysis. Using pulsed laser excitation and a highly diluted aqueous solution of silver colloids Ag54 ($\approx 10^{13}$ particles/L) with an average of less than one Rhodamine 6G per particle, signal bursts with count rates higher than 100 kHz indicate transits of individual particles/molecules. Figure 2A shows the time-gated signal traces (see below), which allow to distinguish between the temporally prompt, *p*, Raman signal (upper trace) and the delayed, *d*, fluorescence signal (lower trace).

Using the excitation by a pulsed, linear polarized laser and a confocal microscope with two detectors, MFD allows us to calculate three spectroscopic parameters from the stored data list: (i) intensity, I_S, related to the interphoton times Δt between signal photons which are measured with a time resolution of 50 ns, (ii) the signal decay characterized by the 1/e-decay time τ_S, which is obtained from signal arrival times measured by time-correlated single-photon counting (TCSPC), and (iii) experimental, time-integrated anisotropy r.[15]

An important step in analyzing a single-molecule experiment is to distinguish between signal and background. Burst selection can nicely be realized using the time information contained in the interphoton time Δt. We classified a signal with a drop of Δt as signal burst if 150 consecutive photons are below the threshold value of 49 μs of the Lee filtered data.[24] This way, data analysis is restricted to only those registered events which are within the signal burst of a single molecule/particle transit selected from the signal trace.

TCSPC allows us to construct histograms of photon arrival times relative to the incident laser pulse for each selected region in the signal trace (histograms 1−4, lower part of Figure 2). Because of the pronounced difference in the decay times, time-gating is an efficient criterion to distinguish between prompt Raman (*p*: channels 20−50) and delayed fluorescence signal (*d*: channels 60−250) in computed multichannel scaler traces (upper/lower trace Figure 2A, the time gating intervals are indicated by arrows in signal arrival time histogram 1 of Figure 2B). Four typical situations are marked in the signal traces (Figure 2A), and the corresponding arrival time histograms aimed to illustrate different signal decay properties are shown in Figure 2B: (1) background signal due to the Raman signal of water and dark counts of the detector (12 kHz, 65% of the total signal appear in the *p*-channels), (2) SERRS bursts with count rates of more than 100 kHz (87% of the signal in the *p* channels), (3) fluorescence signal within a SERRS-burst, and (4) fluorescence burst of a freely diffusing Rh6G. As a first step, we assumed no model function to describe the decay properties of the signal. An established maximum-likelihood estimator was applied to calculate the 1/e-signal decay time τ_S for a total number of channels, $m = 200$, starting from the maximum, channel 30, to channel 230, whereby the channel width T is equal to 49 ps. τ_S is given by the weighted sum of the events, N_i, registered in channel i divided by the total number of number of events N (eq 1).[25]

$$1 + (\exp(-T/\tau_S) - 1)^{-1} - m(\exp(-mT/\tau_S) - 1)^{-1} = N^{-1}\sum_{i=1}^{m} iN_i \quad (1)$$

Single-Molecule/Particle Characterization. The statistical relevance of our single-molecule observations is judged by sliding a signal-parameter analysis of 300 cut bursts to generate parameter-time trajectories.[26] This is achieved by binning the

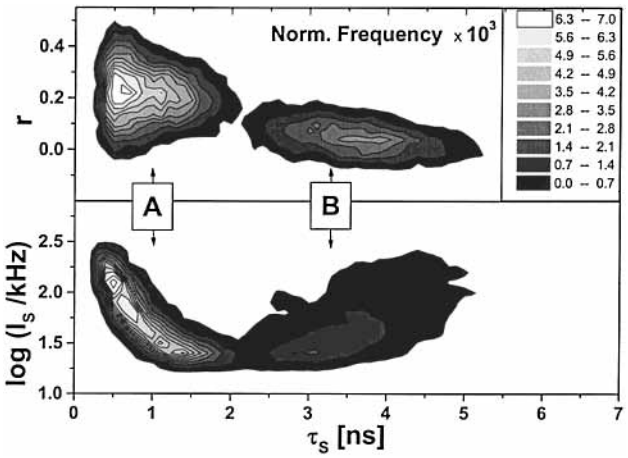

Figure 3. Two-dimensional density maps of the occurrence of parameter pairs: 1/e-signal decay time, τ_S/anisotropy, r (top) and 1/e-signal decay time, τ_S/signal intensity, I_s (bottom). The parameters were obtained by sliding analysis with a photon window of 150 events. τ_S was determined from the channels 30−230 according to eq 1.

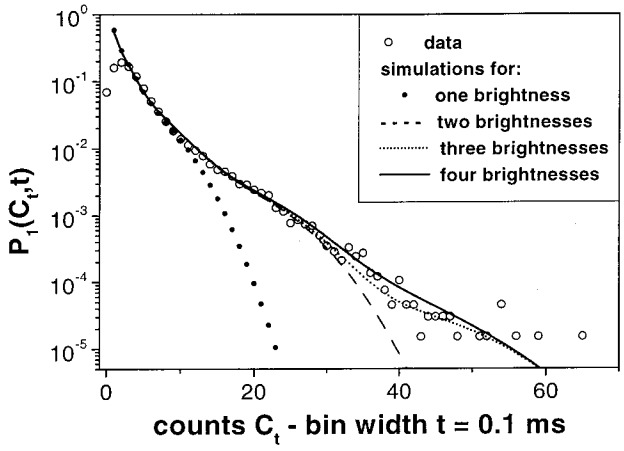

Figure 4. Signal intensity distribution analysis (data, open circles) for bursts of region A in Figure 3. The reduced values for $C_t < 3$ are caused by the burst selection algorithm and are neglected in the simulations. Simulations for the photon count density, $P_1(C_t,t = 100\ \mu s)$, calculated according to eq 9 of ref 17 are based on models with a background signal of 12 kHz (14%) and a varying number of fixed brightnesses: one brightness (black dots), $C_0 = 12$ (86%); two brightnesses (dashed line), $C_0(1) = 12$ (56%) and $C_0(2) = 28$ (30%); three brightnesses (dotted line), $C_0(1) = 12$ (56%), $C_0(2) = 28$ (28%), and $C_0(3) = 56$ (2%); and four brightnesses (solid line), $C_0(1) = 12$ (56%), $C_0(2) = 28$ (26%), $C_0(3) = 40$ (3%), and $C_0(4) = 56$ (1%).

signal inside the bursts into subhistograms with a constant number of events (150). With this event window slid stepwise along the registered events, three parameter traces for signal intensity I_S, 1/e-signal decay time τ_S, and anisotropy r, are calculated. The macroscopic time information of these signal parameter traces is obtained by the mean of the interphoton times Δt. In this way, the time evolution of characteristic parameters of a single molecule/particle can be monitored simultaneously in real time. For each point of time, the values of the r/τ_S and I_S/τ_S pairs are counted to generate a two-dimensional normalized frequency histogram of all cut bursts as shown in Figure 3.

In the Ag54 sample, two different species, adsorbed and free dye marked as regions A and B, are clearly evident in the distributions of the normalized frequency of r/τ_S and I_S/τ_S pairs (Figure 3). Within the error limits of ±17% determined for the sliding analysis window of 150 events, the adsorbed dye (A) is characterized by a prompt, strongly polarized Raman signal (the decay time τ_S is equal to the instrument response function with included background events, the average anisotropy $r_{av} = 0.24$) and the free dye (B) by a well-known, unquenched, mainly depolarized fluorescence ($\tau_S = 3.8$ ns, $r_{av} = 0.02$).[17,18] As expected, for the slowly diffusing silver nanoparticles with a measured FCS diffusion time of $\tau_D = 20$ ms (see discussion below), bursts with more than 2000 registered events fall only in region A. The lower plot of Figure 3 directly proves that under our conditions, where the selected spectral range favors SERRS detection, the Raman scattering signal (>100 kHz) is higher than the fluorescence signal. If, however, the setup is optimized for the detection of Rhodamine 6G fluorescence, I_s values >300 kHz (data not shown) can be obtained, i.e., SERRS and fluorescence can approximately achieve the same signal strengths.

Signal-Intensity Distribution Analysis. Recently a methodology, fluorescence-intensity distribution analysis (FIDA), has been developed by several groups for confocal microscopy studies in which the fluorescence-intensity distribution of a sample with a spatially heterogeneous signal profile is analyzed.[17,27,28] FIDA allows one to determine specific brightness values, C_0, in a heterogeneous sample in dependence on experimental parameters (spatially variable laser intensity $I(r)$, detection efficiency g) and sample characteristics (fluorescence quantum yield, dark state properties, number of bound fluorophores to a single nanoparticle, and the degree of aggregation of single-labeled analyte). In our model, the brightness is a dimensionless value which corresponds to the number of counts in a time interval t, during which the molecule resides in the center of the detection volume element with $I(r = 0)$ (compare eq 9 of ref 17; $C_0 = g\, I(r)\, t$). In the framework of FIDA analysis, the MFD-intensity data shown in Figure 3 (region A) are converted into a probability density, $P_1(C_t,t)$, of fluorescence count rates, C_t, in a certain time interval ($t = 100\ \mu s$) to obtain information on the brightness, $C_0(X)$, of each contributing species X (Figure 4). The increase of experimental $P_1(C_t,t)$ data (open circles) in the first three channels is caused by the use of cut bursts and is not considered in the simulation. The signal intensity density of the bursts in region A is compared with four simulations assuming different numbers of species with fixed brightness values. Thereby $P_1(C_t,t)$ is computed as a normalized sum of poisson-distributed background signal and fluorescence with species-specific brightnesses, $C_0(X)$, (eq 9 of ref 17). The comparison shows that at least three (dotted line) or four brightnesses (solid line), $C_0(1) = 12$ (56%), $C_0(2) = 28$ (26%), $C_0(3) = 40$ (3%), and $C_0(4) = 56$ (1%), and a background of 12 kHz (14%) are necessary to achieve a satisfactory agreement between theory and experiment. In principle, this heterogeneity of the signal can have several reasons such as particle aggregation, more than one SERRS-active molecule adsorbed on the nanoparticle, and different binding sites with specific SERRS enhancement factors. As discussed in detail below, particle aggregation as the main reason for heterogeneity can be excluded by their rotational and translational diffusion characteristics, spectral properties of the colloid (Figure 1A), and results of photon correlation experiments. In view of the applied stoichiometry, binding of multiple dyes on the nanoparticle is not very likely. Accordingly, the low fraction of the large brightnesses, $C_0(3) = 40$ (3%) and $C_0(4) = 56$ (1%), might be attributed to this effect because of a superposition of the lower brightnesses. Therefore, we postulate that the main fraction of the signal, characterized by two brightnesses $C_0(1) = 12$ (56%) and $C_0(2) = 28$ (26%), is predominantly generated by single SERRS active dye molecules in heterogeneous binding sites.

Binding Interactions of Rh6G on Silver Colloids. It is well-known that the fluorescence of dyes adsorbed at a metal surface is quenched by through-space, long-range energy transfer of the Foerster type. On the other hand, SERRS very critically depend on short distances to the surface. For our case of a cationic dye interacting with an anionic colloid, a high chemisorption energy of 65 kJ/mol was reported by ref 21. This is also in agreement with the results presented in Figures 3 and 4, which provide no evidence for a significant population of a third species of weakly bound dye molecules simultaneously showing fluorescence and Raman signal. Let us, however, investigate the question whether there exists a diffuse layer surrounding the colloids, where in rare events locally diffusing Rh6G molecules exhibit intermediate properties because of weak contact: shortened fluorescence lifetimes and little or no SERRS.

The inspection of the time-gated signal traces of all 330 Ag54 SERRS bursts (Figure 2) shows the occurrence of rare events (21 bursts = 6%) characterized by a fluorescence burst inside a SERRS burst (as illustrated in histogram 3) with more than 80 delayed events in a time interval of a few milliseconds. Such an observation can be explained either by a simultaneous transit of a SERRS active colloid and a free dye or by the above proposal of a single Ag particle with a Rh6G molecule in weak contact. Seeing that such rare events are hidden in the broad ensemble-averaged distribution of Figure 3, a more detailed decay analysis of individual selected bursts was performed to obtain the fluorescence lifetime τ_F and the rotational correlation time ρ for a selected region of fluorescence bursts inside a SERRS burst. As described in ref 18, a pattern recognition algorithm was applied to globally analyze the ungated signal of the detectors [parallel (x) and perpendicular (y)] and to describe the signal I_S by a sum of fluorescence and background signal I_B, which yields also the fraction of I_B, $\gamma = I_B/I_S$ (bold lines in the histograms 3 and 4 of Figure 2B). If in a control experiment a sample with only free dye molecules is analyzed in this way, we obtain a distribution of fluorescence lifetimes with a width predicted by statistics: $\tau_F = 4.0 \pm 0.6$ ns, i.e., only 5% of all dye bursts will have a $\tau_F < 2.9$ ns (e.g., Figure 2B histogram 4; $\tau_F = 4.1 \pm 0.4$ ns and $\rho = 0.2 \pm 0.1$ ns).[17] However, if we analyze only those 21 bursts of the Ag54 sample, which simultaneously show a fluorescence and SERRS signal, 11 of these fluorescence bursts (i.e., 50%) have a polarized and more or less quenched fluorescence (e.g., Figure 2 histogram 3; $\tau_F = 2.9 \pm 0.35$ ns and $\rho = 0.7 \pm 0.1$ ns). This fraction of 50% of the Ag54 sample is 10-times higher than the fraction of 5% expected from the control experiment with the free dye. The statistically significant evidence of a simultaneous SERRS and fluorescence signal in rare events allows one to detect the existence of a diffuse layer as an intermediate and locally and temporally limited case, where Rh6G molecules only weakly interact with the metal surface in a somewhat larger distance.

Ensemble and Selective Autocorrelation Analysis. The dynamic behavior of the Raman signal was analyzed by calculating the normalized autocorrelation function $G_N(t_c)$, with the correlation time t_c (eq 2).

$$G_N(t_c) = \frac{\langle N_s(t)\, N_s(t+t_c)\rangle}{\langle N_s(t)\rangle^2} = 1 + \frac{\langle \delta N_s(t)\, \delta N_s(t+t_c)\rangle}{\langle N_s(t)\rangle^2} \qquad (2)$$

Here, N_S signifies the photon counts in a time interval T_S, and the temporal dependence of the signal $N_S(t) = \langle N_S(t)\rangle + \delta N_S(t)$ is described by the signal fluctuations signal $\delta N_S(t)$ about its mean $\langle N_s\rangle$ ($\langle\rangle$ denotes time averaging over the real time, t).

The analysis of the autocorrelation curve of the ensemble (average over the whole signal of the heterogeneous sample solution, data not shown) yields a characteristic diffusion time $\tau_D = 20$ ms. This time corresponds closely to the diffusion time expected for a sphere with a radius of 27 nm calculated by the Stokes−Einstein equation.[6] This indicates that under our experimental conditions trapping of the colloids by the laser beam is not significant. Evidence for the lack of aggregation is also given by previous experiments employing the photon correlation technique which showed that the particle diameters derived for nonaggregated particles via the Stokes−Einstein equation match very well those determined by transmission electron microscopy.[22,23]

For selective autocorrelation analysis, a signal trace giving the number of events $N_S(t = iT_S)$, in the time interval $[iT_S] \le t < [(i+1)T_S]$, is calculated from the interphoton times Δt. Analyzing a measurement with a total number of K cut bursts, signal traces with M_n time intervals of the length T_S are computed for each burst for $n = 1$ to K. Hence, the individual burst duration time is given by $T_n = M_n T_S$. The normalized autocorrelation function $G_N(t_c = jT_S)$ (eq 2) is calculated by temporally averaging over all i values, $N_S(t) = N_S(iT_S)$, in a burst and over all bursts N ($\langle\,\rangle$ in eq 2). Before normalization of $G_N(t_c = jT_S)$ according to eq 2, the numerator and denominator of G_N are computed separately over all K bursts for each correlation time, $t_c = jT_S$, as defined in eq 3.

$$\langle N_S(t)N_S(t+t_c)\rangle = \frac{1}{\sum_{n=1}^{K} M_n - j} \sum_{n=1}^{K} \sum_{i=0}^{M_n - j - 1} N_S(iT_S)N_S(iT_S + jT_S)$$

$$\text{for } (t_c = jT_S)$$

$$\langle N_S(t)\rangle = \frac{1}{\sum_{n=1}^{K} M_n} \sum_{n=1}^{K} \sum_{i=0}^{M_n - 1} N_S(iT_S) \qquad (3)$$

Autocorrelation curves, $G_N(t_c)$, were computed for the gated prompt Raman signal with parallel p_x, perpendicular p_y, and nonpolarized detection p_{x+y} and for the total signal without time gating, *all* (Figure 5).

Table 1 summarizes the analysis of these curves using the fit function $G_N(t_c) = \sum_i A_i \exp(-t_c/t_i) + c$, consisting of a sum of bunching terms with the amplitudes A_i and characteristic correlation times t_i. The residuals (lower part of Figure 5) and the values of χ^2 indicate that four exponentials are necessary to describe the decay over three time decades: (1) three bunching times in the microsecond time range differing by a factor of 5−6 and (2) a forth exponential in millisecond time range to approximate the translational diffusion term which is distorted by the cutting. The increased total correlation amplitude of G_N-(p signal) compared to G_N(all signal) in Figure 5 proves that the signal-to-background ratio in the signal traces is indeed improved by time gating. Furthermore, the total amplitude of $G_N(t_c)$ and especially the amplitudes A_1 and A, strongly depend on the polarization.[29] This leads to the assumption that the bunching terms $A_1(t_1)$ and $A_2(t_2)$ reflect the rotation of a particle, because it is well-known from FCS theory that a spherical rotor induces intensity fluctuations leading to strongly polarization dependent autocorrelation curves. For the case of a spherical rotor, FCS theory predicts two rotational bunching times t_1 and t_2 in the correlation curve which are connected to a single rotational correlation time ρ via $t_1 = \rho/3.3$ and $t_2 = \rho$.[30] Under

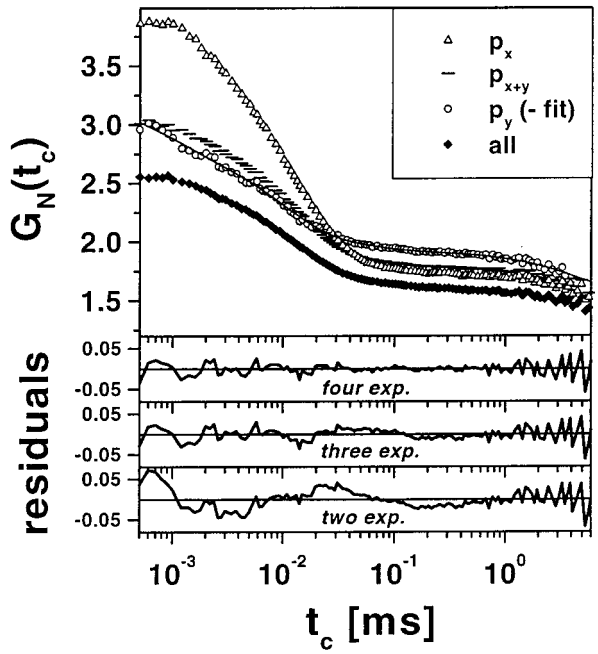

Figure 5. Normalized autocorrelation curves, $G_N(t_c)$, calculated from different signal components: entire signal (all) and prompt signal with polarization, parallel (p_x) or perpendicular (p_y), and unpolarized (p_{x+y}). In addition, a fit to p_y including four exponential terms (details see text) is shown (solid line). The residuals of the fits to this individual measurement including four (top), three (middle), and two (bottom) exponential terms are also shown below. Fit parameters for four exponentials: $c = 1.53$, $A_1 = 0.30$, $t_1 = 0.9$ μs, $A_2 = 0.72$, $t_2 = 9.6$ μs, $A_3 = 0.16$, $t_3 = 40$ μs, $A_4 = 0.39$, $t_4 = 5.0$ ms, and $\chi^2 = 0.034$. For three exponentials: $c = 1.60$, $A_1 = 0.44$, $t_1 = 1.4$ μs, $A_2 = 0.78$, $t_2 = 14.0$ μs, $A_3 = 0.34$, $t_3 = 3.4$ ms, and $\chi^2 = 0.042$. For two exponentials: $c = 1.65$, $A_1 = 0.98$, $t_1 = 9.7$ μs, $A_2 = 32$, $t_2 = 2.4$ ms, and $\chi^2 = 0.089$. In the fits, the applied weighting factor was the inverse of the $G_N(t_c)$.

TABLE 1: Selective Autocorrelation Analysis of Ag54−SERRS bursts Yielding Three Bunching Times, $t_{1,2,3}$, in Addition to a Forth Exponential Approximating the Translational Diffusion Term

Ag54	t_1 (A_1) [μs]	t_2 (A_2) [μs]	t_2/t_1	A_2/A_1	t_3 (A_3) [μs]
p_{x+y}[a]	2.0 (0.16)	13 (1.04)	0.15	6.5	64 (0.11)
p_x[a]	4.0 (0.52)	15 (1.62)	0.27	3.1	59 (0.13)
p_y[b]	1.3 (0.29)	10 (0.70)	0.13	2.4	37 (0.17)
all[a]	2.3 (0.16)	14 (0.76)	0.16	4.8	78 (0.10)

the assumption of parallel absorption and emission dipoles, theory predicts a strong polarization dependence for the amplitude ratio, namely, $A_2/A_1 = 23$ (p_{x+y}), 11.3 (p_x), and 0.6 (p_y).[30] In our case, where the signal originates from inelastic light scattering, we can expect that the relationship derived for the two rotational bunching times is conserved, whereas the amplitude ratio for different experimental conditions (p_{x+y}, p_x, and p_y), which describes the (de)polarization characteristics of the signal, can be slightly modified because of nondiagonal terms in the scattering tensor. On the basis of the FCS model, we must interpret the second bunching time t_2 as the "actual" rotational correlation time ρ of the silver particles with a diameter $d = 54$ nm. Applying the Stokes equation, $\rho = \eta\pi d^3/6kT$, for water (viscosity, $\eta = 1$ cP; sphere diameter $d = 54$ nm; temperature, $T = 300$ K; and $k =$ Boltzmann constant), we obtain a rotational correlation time of $\rho = 18$ μs, which is in good agreement with t_2 given in Table 1. The values determined for the first bunching time t_1 are, considering the different accuracy because of different levels of signal and uncorrelated background in p_x and p_y, close to the ratio, t_2/t_1, of 0.3 expected from theory. This qualitative agreement indicates that t_1 also reflects the rotation of the SERRS-active silver particles and is, therefore, not indicative for a different process. In favor of the given interpretation is also the ordering of the amplitude ratios $A_2/A_1(p_{x+y}) > A_2/A_1(p_x) > A_2/A_1(p_y)$. We conclude that the rotational and translational diffusion properties of Ag54 give confidence for the observation of only single, approximately spherical, SERRS-active silver particles and exclude the dominant contribution from aggregates. Of course, it cannot be excluded that the ensemble of particles, not being perfectly round and of exactly the same size, needs the consideration of more than one rotational correlation time for a perfect modeling. The mentioned photon correlation measurements showed, however, that for our colloid preparation restriction to one component yields a satisfactory interpretation of the experimental results. Here again, the advantage of using monodisperse colloids shows up, because already dimer formation causes a large relative change of the characteristic relaxation times. The dimer formation would result in particles with the shape of a prolate, which causes an increase of the mean rotational correlation time ρ from 18 to 32 μs. However, this process can be ruled out, because signal fluctuations in this time regime are not observed in the autocorrelation curves.

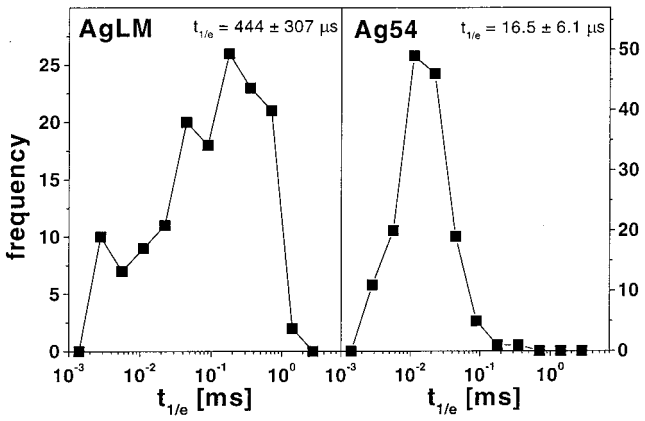

Figure 6. Frequency histogram of the mean rotational relaxation times, $t_{1/e}$, obtained from the p_{x+y} autocorrelation curves of 154 individual Ag54 and Ag147 individual AgLM bursts. In the histogram, only those SERRS bursts are considered which have an amplitude $A > 0.01$ of the rotational relaxation time, $t_{1/e}$. The mean values and standard deviations are obtained by a fit of a Gaussian distribution to the data (fit not shown).

Compared to the other amplitudes, the amplitude of the third bunching time, $t_3 \approx 60$ μs, is less polarization dependent, which may be an indication for a dynamic process influencing the SERRS enhancement of the chromophore. One plausible explanation is local movements of the dye at the binding site changing their adsorption geometry relative to the metal surface and, therefore, their efficiency of the SERRS signal. The existence of heterogeneous binding sites with specific brightnesses is also supported by the FIDA measurements of Figure 4.

Single-Particle Autocorrelation Analysis. The usefulness of MFD for single-particle analysis is demonstrated in Figure 6. To study directly the heterogeneity of the rotational behavior of the silver colloids, autocorrelation analysis of the p_{x+y} signal in each single SERRS burst was performed to characterize the rotational properties of each individual particle by a single mean rotational relaxation time, $t_{1/e}$, of the individual autocorrelation curve. Two samples are compared: the monodisperse Ag54 and the polydisperse and larger AgLM. The determined average value and the standard deviation of the frequency histograms,

$t_{1/e}$(Ag54) = 16.5 ± 6.1 μs and $t_{1/e}$(AgLM) = 444 ± 307 μs, reveal an increase in size and heterogeneity of the polydisperse sample AgLM. These results are in perfect accordance with the heterogeneity of sizes and shapes of Ag particles in both preparations as measured by electron microscopy.[19]

In summary, this letters reports the first SERRS correlation spectroscopy of single dye molecules on single particles in solution by applying the MFD technique. MFD allowed us direct identification of individual particles/molecules in a heterogeneous sample via their characteristic signal decay time, anisotropy, brightness, and rotational diffusion time. The consistent results of FIDA (Figure 4), rotational correlation times (Figure 6), and previous work [22] are in accordance with well defined nonaggregated Ag54 particles. For the sample Ag54, this contradicts the hypothesis that colloid aggregation is indispensable for achieving high SERRS amplification factors. With the awareness that a single Ag particle has a distinctly faceted shape with tips, wedges, and cavities, the prediction of the SERS quadrupole theory[16] is in line with our observation that the enhancement may reach enormous values in the range of 10^{10}–10^{16} for dye molecules attracted by such "hot" spots. The applied preparation protocol allows us to reproducibly synthesize small, monodisperse Ag crystals with a high SERRS activity. Thereby, the size of 54 nm is approximately half of that of the particles used in previous work.[3,5,12] However, one has to keep in mind that the optimum excitation wavelength for SERRS varies with the plasmon absorption band, which in turn is dependent on particle size and dielectric constant of the surrounding medium.

Several indications for a dynamic interchange between binding sites have been provided: (1) blinking behavior of single particles in the sub-second time range,[12] (2) multiple brightnesses observed by FIDA indicative for heterogeneous sites, (3) autocorrelation analysis revealed a fast blinking behavior in the time range of 60 μs, which may be attributed to local movements of the dye around a specific binding site, and finally, (4) selective analysis of rare events allowed for the detection of a small population of a weakly fluorescent and less mobile Rh6G species, which is assumed to have a larger distance to the metal surface. This detection of rare events is hidden in an ensemble-averaged analysis (Figure 3) and can only be revealed by the analysis of single events using MFD.

Acknowledgment. Financial support by DFG, VW Foundation, BMBF, and FdCh is gratefully acknowledged. We thank F. Keilmann, A. Volkmer, and E. Haustein for stimulating discussions.

References and Notes

(1) Moerner, W. E.; Kador, L. *Phys. Rev. Lett.* **1989**, *62*, 2535−2538.

(2) Orrit, M.; Bernard, J. *Phys. Rev. Lett.* **1990**, *65*, 2716−2719.

(3) Nie, S.; Emory, S. R. *Science* **1997**, *275*, 1102−1106.

(4) Xu, H. X.; Bjerneld, E. J.; Kall, M.; Borjesson, L. *Phys. Rev. Lett.* **1999**, *83*, 4357−4360.

(5) Kneipp, K.; Wang, Y.; Kneipp, H.; Perelman, L. T.; Itzkan, I.; Dasari, R. R.; Feld, M. S. *Phys. Rev. Lett.* **1997**, *78*, 1667−1670.

(6) Magde, D.; Elson, E. L.; Webb, W. W. *Phys. Rev. Lett.* **1972**, *29*, 705−708.

(7) Eigen, M.; Rigler, R. *Proc. Natl. Acad. Sci. U.S.A.* **1994**, *91*, 5740−5747.

(8) Ehrenberg, M.; Rigler, R. *Chem. Phys.* **1974**, *4*, 390−401.

(9) Widengren, J.; Rigler, R. *Cell. Mol. Biol.* **1998**, *44*, 857−879.

(10) Schrof, W.; Klingler, J. F.; Rozouvan, S.; Horn, D. *Phys. Rev. E* **1998**, *57*, 2523−2526.

(11) Kneipp, K.; Kneipp, H.; Itzkan, I.; Ramachandra, R. D.; Feld, M. S. *Chem. Rev.* **1999**, *99*, 2957−2975.

(12) Michaels, A. M.; Nirmal, M.; Brus, L. E. *J. Am. Chem. Soc.* **1999**, *121*, 9932−9939.

(13) Krug, J. T.; Wang, G. D.; Emory, S. R.; Nie, S. M. *J. Am. Chem. Soc.* **1999**, *121*, 9208−9214.

(14) Zenobi, R.; Deckert, V. *Angew. Chem.* **2000**, *39*, 1746−1756.

(15) Kneipp, K.; Harrison, G. R.; Emory, S. R.; Nie, S. M. *Chimia* **1999**, *53*, 35−37.

(16) Polubotko, A. M. *J. Opt. A: Pure Appl. Opt.* **1999**, *1*, L18−L20

(17) Fries, J. R.; Brand, L.; Eggeling, C.; Köllner, M.; Seidel, C. A. M. *J. Phys. Chem. A* **1998**, *102*, 6601−6613.

(18) Schaffer, J.; Volkmer, A.; Eggeling, C.; Subramaniam, V.; Striker, G.; Seidel, C. A. M. *J. Phys. Chem. A* **1999**, *103*, 331−336.

(19) Schneider, S.; Halbig, P.; Grau, H.; Nickel, U. *Photochem. Photobiol.* **1994**, *60*, 605−610.

(20) Shirtcliff, N.; Nickel, U.; Schneider, S. *J. Colloid Interface Sci.* **1999**, *211*, 122.

(21) Hildebrandt, P.; Stockburger, M. *J. Phys. Chem.* **1984**, *88*, 5935−5944.

(22) Grau, H. Ph.D. Dissertation, University Erlangen−Nuernberg, 1995.

(23) Gliemann, H. Ph.D. Dissertation, University Erlangen−Nuernberg, 1999.

(24) Enderlein, J.; Robbins, D. L.; Ambrose, W. P.; Goodwin, P. M.; Keller, R. A. *Bioimaging* **1997**, *5*, 88−98.

(25) Hall, P.; Selinger, B. *J. Phys. Chem.* **1981**, *85*, 2941−2946.

(26) Eggeling, C.; Fries, J. R.; Brand, L.; Günther, R.; Seidel, C. A. M. *Proc. Natl. Acad. Sci. U.S.A.* **1998**, *95*, 1556−1561.

(27) Chen, Y.; Müller, J. D.; So, P. T. C.; Gratton, E. *Biophys. J.* **1999**, *77*, 553−567.

(28) Kask, P.; Palo, K.; Ullmann, D.; Gall, K. *Proc. Natl. Acad. Sci. U.S.A.* **1999**, *96*, 13756−13761.

(29) Kask, P.; Piksarv, P.; Pooga, M.; Mets, Ü.; Lippmaa, E. *Biophys. J.* **1989**, *55*, 213−220.

(30) Aragón, S. R.; Pecora, R. *Biopolymers* **1975**, *14*, 119−138.